International Journal of Thermophysics, Vol. 5, No. 2, 1984

Thermophysical Properties of Molten Salts: Hypersonic Velocities of Molten Alkali Nitrates and Their Mixtures[1]

T. Ejima[2] and T. Yamamura[2]

Received February 8, 1984

By means of Brillouin scattering spectroscopy, hypersonic velocities in $NaNO_3$–KNO_3 binary melts have been measured at temperatures from the liquidus temperatures of the melts to 200 K above them over the entire range of compositions. The light beam scattered by the melt is analyzed with a pressure-scanned Fabry–Perot spectrometer. The hypersonic velocities obtained are about the same as the ultrasonic velocities reported at compositions rich in $NaNO_3$, but are markedly larger than those at compositions rich in KNO_3, indicating the occurrence of structural relaxation. Thermodynamic values such as adiabatic and isothermal compressibilities, constant-volume heat capacity, and internal pressure calculated from the sound velocity obtained show that the melt can be treated as a typical ionic liquid, though it contains a certain amount of associated species.

KEY WORDS: alkali nitrates; Brillouin scattering; mixtures; molten salts; thermophysical properties.

1. INTRODUCTION

Much of the interest in molten salt chemistry over the last decade or two has arisen from the needs of high-temperture technology, primarily those related to extractive metallurgy of light metals, molten salt breeder reactor development, reactor fuel processing, development of molten salt batteries, and fuel cell, heat exchange, or heat storage media.

[1] Paper presented at the Japan–United States Joint Seminar on Thermophysical Properties, October 24–26, Tokyo, Japan.

[2] Department of Metallurgy, Tohoku University, Sendai, Japan.

0195-928X/84/0600-0131$03.50/0

Molten salts are a special class of liquid, comprised entirely of positively and negatively charged ions undiluted by a weak electrolyte supporting medium. When dealing with physicochemical properties of a general liquid an equation of state becomes of fundamental importance. However, in the case of a molten salt, the constituent particles, such as ions of positive and negative charge, holes, ion pairs or ion-associated groups, complex ions, and molecules, become more important than the equation of state because of the interactions that exist among the constituent ions.

Physicochemical properties of molten salts are more or less affected by the kinds of existing species and the interactions among the constituent ions. The transport properties are particularly structure sensitive compared with the other properties. Electrical conductance, which is the coefficient representing the charge transfer process, depends mainly on the small cations, and shear viscosity, which is the coefficient representing the momentum transfer process, is affected largely by the anions or complex ions having a size larger than the cations. Diffusivity for the mass transfer process is influenced by the number and size of holes in the molten salt, which are introduced in the process of melting and paired ions. Sound velocity, compressiblity and bulk (volume) viscosity, which are the coefficients representing the sonic energy transfer process, are sensitive to the ionic species.

One of the most effective ways to obtain information about the structure of molten salts and to evaluate the nature and range of such interactions is to measure the temperature and composition dependences of transport properties precisely. Sonic spectroscopy is one of the most effective methods of detecting the existence of associated species in liquids. Much work has been done on the temperature and composition dependences of ultasonic velocity in common liquids, but few results have appeared [1, 2] for molten salts, because of experimental difficulties.

The absorption of sound energy by a liquid medium is attributed to the shear viscosity, which is the resistivity for the structural deformation resulting from the shear stress applied to the fluid, and the bulk viscosity, which is the resistivity to the volumetric change at the time the liquid expands or contracts to the volume in equilibrium with the external pressure. Bulk viscosity can be determined by measuring the attenuation of a sound wave when a cyclic pressure change is applied to the liquid with high-frequency sound waves so as to bring about compression and expansion. Usually, an ultrasonic wave is used to provide such a cyclic pressure change to the liquid. The highest frequency of ultrasonic wave applicable to the measurement of bulk viscosity is limited to 400 MHz, because the absorption of a sound wave by a liquid medium increases as the frequency of ultrasound increases in the case of high-temperature molten salts.

For $NaNO_3$–KNO_3 binary melts, there are linear relations between the composition and such transport properties as electrical conductance and shear viscosity. Furthermore, heats of mixing of the binary melts show extremely small negative values. These facts may suggest that the $NaNO_3$–KNO_3 binary melt can be treated as an ideal mixture. However, the structure of a molten alkali nitrate is not as simple as a typical ionic melt such as an alkali chloride because of the existence of associated species as observed by neutron diffraction analysis [3]. For alkali nitrates, the dispersion of sound propagation caused by the structural relaxation of associated species has not been measured by ultrasonic spectroscopy. The relaxation may take place in a frequency range much higher than that of ultrasound, probably in the gigahertz region.

Sonic spectroscopy in the gigahertz region becomes possible if Brillouin scattering is applied. In the present study, hypersonic velocities in molten single salts of $NaNO_3$, KNO_3, and $NaNO_3$–KNO_3 binary melts have been measured by means of the Brillouin scattering method over the frequency range of 2–7 GHz. The hypersonic velocities obtained were compared with the ultrasonic velocities found in the literature to check whether or not the relaxation takes place in the frequency range studied. Thermodynamic values such as adiabatic and isothermal compressibilities, constant-volume heat capacity, and internal pressure were calculated from the hypersonic velocities determined.

2. METHOD

As predicted by Brillouin [4] in 1914, the light scattered by a homogeneous liquid consists of a central Rayleigh line with the same frequency as that of the incident beam, and a doublet of which the components are shifted symmetrically from the frequency of the incident beam. The latter is induced by the collision of a photon and a phonon in the liquid under thermal equilibrium. The frequency shift $\Delta\nu$ between the Brillouin peaks and the Rayleigh peak is expressed as follows:

$$\Delta\nu = +2\nu_i n(V_s/c)\sin\theta \tag{1}$$

where ν_i is the frequency of the incident beam, n is the refractive index of the liquid, V_s and c are the velocities of sound and light, and θ is the scattering angle. The sound velocity V_s can be obtained from the frequency shift and the measured scattering angle. If it is assumed that the propagation of sound proceeds adiabatically and that local fluctuation of liquid density due to the propagation of sound is negligibly small, such thermodynamic values as adiabatic compressibility β_s, isothermal compressibility β_t,

constant-volume heat capacity C_v, and internal pressure P_{int} can be calculated from the determined sound velocity with the equations

$$\beta_s = 1/\rho V_s^2 \tag{2}$$

$$\beta_t = \beta_s + TV\alpha^2/C_p \tag{3}$$

$$C_v = C_p\beta_s/\beta_t \tag{4}$$

$$P_{int} = T\alpha/\beta_t \tag{5}$$

where ρ is the density of the liquid, T is the absolute temperature, V is the molar volume of the liquid, α is the thermal expansion coefficient, and C_p is the constant-pressure heat capacity.

The spatial attenuation of the acoustic wave in a liquid, that is, the absorption coefficient of a sound wave γ, is related to the broadening of the Brillouin line, Γ_B, which is expressed by the following equation:

$$\Gamma_B = \gamma V_s/2\pi \tag{6}$$

The hypersonic attenuation γ_s due to the shear viscosity η_s, which is called Stokes' absorption coefficient, is given as follows:

$$\gamma_s = 8\pi^2\nu^2\eta_s/3\rho V_s^3 \tag{7}$$

The hypersonic absorption observed is considerably larger than that predicted by Eq. (7), and this is accounted for by assuming the existence of a bulk viscosity term η_B in addition to the shear viscosity:

$$\gamma = 2\pi^2\nu^2(\tfrac{4}{3}\eta_s + \eta_B)/\rho V_s^3 \tag{8}$$

From the absorption coefficient of sound wave obtained from the measured broadening of the Brillouin component γ_{exp}, it is possible to calculate the bulk viscosity if the shear viscosity is known:

$$\eta_B = \tfrac{4}{3}\eta_s[(\gamma_{exp}/\gamma_s) - 1] \tag{9}$$

In the present investigation, the bulk viscosity has not been calculated because the light source used was not sufficiently monochromatic to provide an accurate measurement of the broadening.

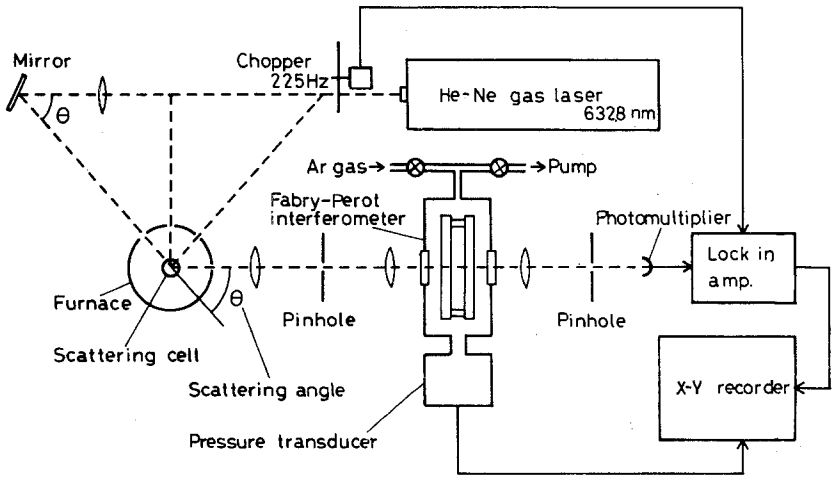

Fig. 1. Experimental arrangement for Brillouin scattering measurement.

A schematic diagram of the experimental apparatus used for the measurement of Brillouin scattering is shown in Fig. 1. The system is composed of a light source, a high-temperature cell, and interferometer, a signal detector, and a recorder. In order to meet the requirement of a coherent and sufficiently monochromatic exciting light, a He–Ne gas laser with power of 50 mW made by Nippon Electric Company is used as the light scource.

The scattering angle and the frequency shift between the Brillouin peaks and the Rayleigh peak were measured by the following procedure. The light from a He–Ne gas laser is modulated to 225 Hz by the use of an optical chopper as shown in Fig. 1. The modulated light is then focussed upon the sample cell placed in an electric furnace. The light scattered at an angle of θ is focussed on a pin hole with a collecting lense and is collimated with a collimating lens. The collimated light is projected to the Fabry–Perot interferometer at a right angle to the etalon plate. The light passed through the interferometer is focussed on a pin hole and is then changed into electrical signals with a photomultiplier. The signals are selectively amplified with a phase-sensitive amplifier and are introduced to an X–Y recorder.

The sound velocity was determined by the following procedure. The spacings between Rayleigh, Stokes, and anti-Stokes peaks are measured and the free spectral range ν_{FSR}, which is the spacing between the Stokes peak and the Stokes peak of the next interferometric order, is determined

from the averaged values of the measured spacings. The frequency shift $\Delta\nu$ is determined by averaging the measured spacings from the Stokes and anti-Stokes peaks to the central Rayleigh peak. On the other hand, the theoretical free spectral range ν_{FSR}(Theor) is calculated from

$$\nu_{FSR}(\text{Theor}) = c/(2n't\cos\varphi) \tag{10}$$

where n' is the refractive index of argon in the etalon plates, t is the spacing of the etalon plates, and φ is the incidence angle of the light beam to the etalon plate. The Brillouin shift $\Delta\nu$ is equal to the product of the observed ratio of $\Delta\nu(\text{Obs})/\nu_{FSR}(\text{Obs})$ and the theoretical free spectral range ν_{FSR}(Theor) given by Eq. (10). The sound velocity with the same frequency as that of the incident beam can be calculated if the determined Brillouin shift is substituted into Eq. (1). The frequency dependence of the sound velocity is also determined by measuring the Brillouin shifts at different scattering angles. In the present study, measurements of Brillouin shifts were made twice at a certain scattering angle, and the mean was taken as the sound velocity at that frequency.

Reagent-grade $NaNO_3$ and KNO_3 are dried at 393 K for 24 h *in vacuo*. The mixture of $NaNO_3$ and KNO_3 is melted in an argon atmosphere and filtered through a sintered Pyrex glass disk to remove small suspended inclusions. The filtrate is poured into a cylindrical cell made of Pyrex glass, and the cell is sealed under vacuum after being cooled. The sample used for the measurement of the Brillouin shift is subjected to quantitative analysis for sodium by the atomic absorption method and for potassium by flame photometry.

3. EXPERIMENTAL RESULTS AND DISCUSSION

3.1. Hypersonic Velocities in Molten $NaNO_3$, KNO_3, and $CsNO_3$

Frequency shifts of Brillouin peaks for molten $NaNO_3$, KNO_3, and $CsNO_3$ were measured over the temperature range from their melting points to 820 K at scattering angles of 48.4, 86.6, and 135.8 deg. Hypersonic velocities calculated from the observed frequency shifts are in good agreement with those reported by Torell and Knape [5] within a difference of 0.8% as shown in Figs. 2–4. A frequency dependence of hypersonic velocity is not observed in the frequency ranges of 2–7 GHz for $NaNO_3$ and KNO_3 and 3–8 Ghz for $CsNO_3$.

The hypersonic velocities obtained were plotted against temperature and are shown in Figs. 4 and 5 compared with ultrasonic velocities found in the literature. As shown in Fig. 4, hypersonic velocities in $NaNO_3$ agree well with ultrasonic velocities determined by Cerisier *et al.* [6] within the

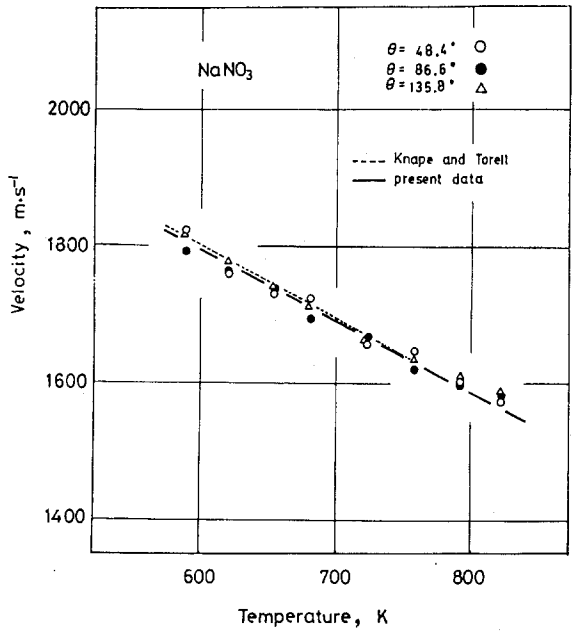

Fig. 2. Temperature dependence of hypersonic velocity for molten $NaNO_3$.

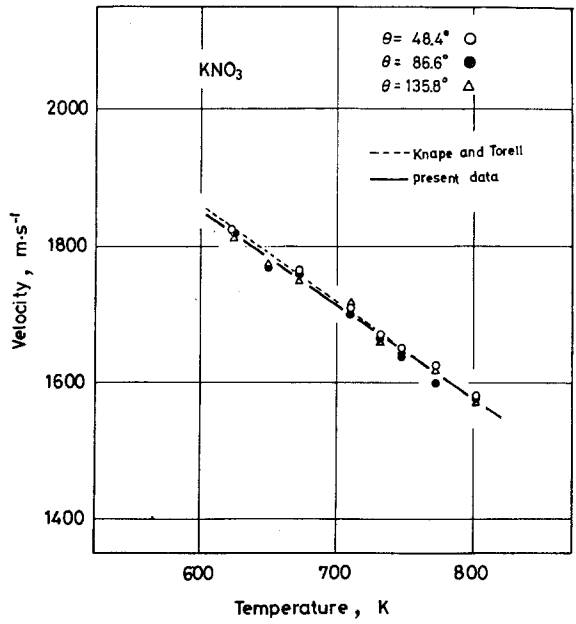

Fig. 3. Temperature dependence of hypersonic velocity for molten KNO_3.

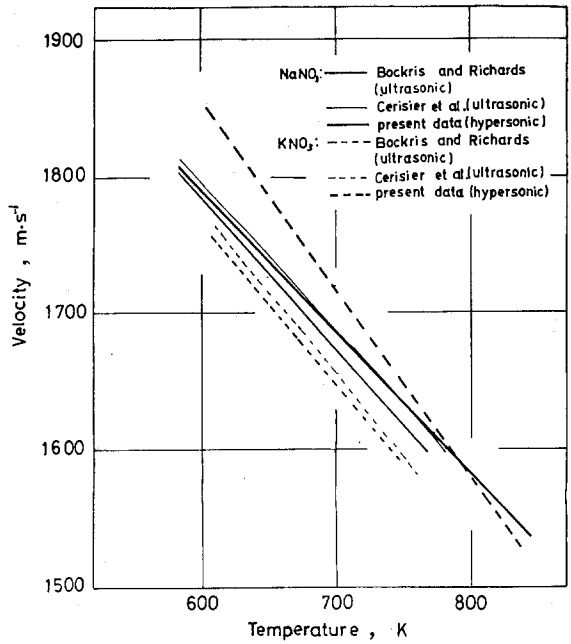

Fig. 4. Temperature dependence of ultrasonic and hypersonic velocities for molten $NaNO_3$ and KNO_3.

limits of experimental error, indicating that the dispersion of sound propagation caused by the structural relaxation of associated species does not occur in the hypersonic and ultrasonic regions. On the other hand, hypersonic velocities in molten KNO_3 are approximately 5% larger than ultrasonic velocities measured by Cerisier *et al.* [6] and Bockris and Richards [7]. Hypersonic velocities in $CsNO_3$ are also approximately 4% larger than ultrasonic velocities measured by Moret [8], as shown in Fig. 5. Such a large difference between hypersonic and ultrasonic velocities beyond the limits of experimental error evidently shows that the dispersion of the sound propagation takes place in the region between the frequencies of ultrasonic and hypersonic waves. From the results obtained, it can be concluded that the relaxation frequency of $NaNO_3$ is more than 7 GHz and those of KNO_3 and $CsNO_3$ are less than 2 and 3 Ghz, respectively.

Since the dispersion of sound propagation was observed in $CsNO_3$, detailed consideration has been given to the relaxation behavior under the assumption that relaxation with a single relaxation time, which has been successfully applied to some molten salts by Knape and Torel [5], can also be applied to the present results. An equation for a static bulk viscosity η_B^0

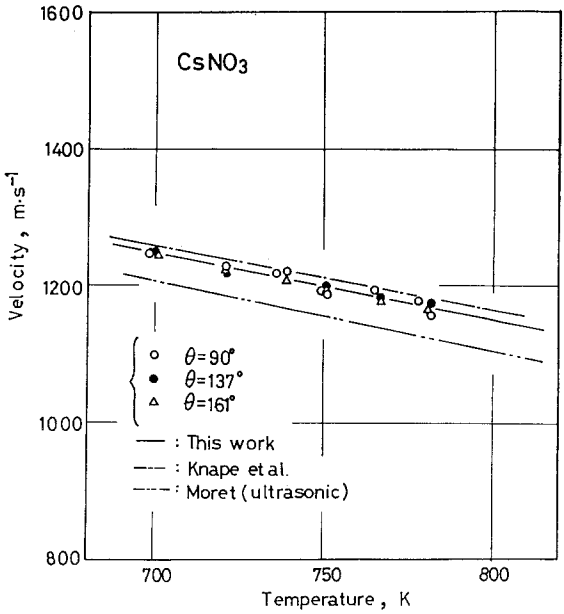

Fig. 5. Temperature dependence of sound velocity in molten $CsNO_3$.

was derived by Montrose *et al.* [9],

$$\eta_B^0 = \rho/(V_\infty^2 - V_0^2)\tau \tag{11}$$

where ρ is the density of the medium, τ is a relaxation time, and V_∞ and V_0 are the sound velocities at the limiting high and low frequencies, respectively. The relaxation time was calculated from the ultrasonic velocity reported by Moret [8] for the values of V_0 and the hypersonic velocity obtained for V_∞. The value obtained is 1.4×10^{-10} s at 731 K.

According to the theory on the basis of single relaxation, the ratio of the absorption coefficient of sound propagation α to the square of the frequency f can be given by

$$\frac{\alpha}{f^2} = \frac{2\pi^2}{\rho V_0^3}\left(\frac{4}{3}\eta_s + \frac{\eta_B^0}{1 + 4f^2\pi^2\tau^2}\right) \tag{12}$$

where η_s is the shear viscosity of the medium. The ratio α/f^2 calculated from the relaxation time obtained is plotted against the logarithm of

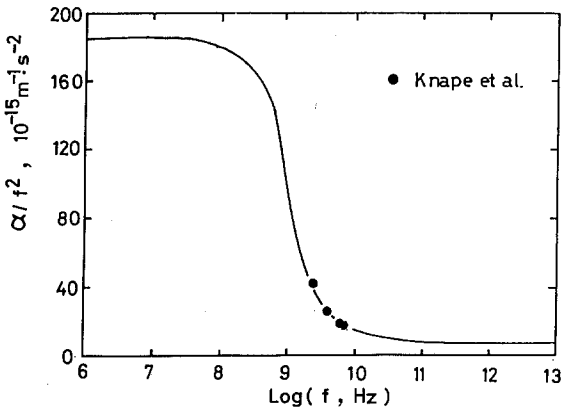

Fig. 6. Plot of α/f^2 versus $\log f$ for molten $CsNO_3$ at 731 K. The solid line represents the theoretical values based on a theory with a single relaxation time. The relaxation time is determined by the use of the velocity measured by this work.

frequency in Fig. 6. The curve agrees very well with the values determined by Knape and Torell [5] on the basis of absorption coefficient measurements.

The temperature dependence of the sound velocities at limiting high and low frequencies is shown in Fig. 7 and compared with each other. Velocities at the high-frequency limit of KNO_3 and $CsNO_3$ and at the low-frequency limit of $NaNO_3$ shown in Fig. 7 are the values obtained in this work. The others were taken from the literature. To obtain the sound velocity at limiting high frequency of $LiNO_3$, the relaxation time was determined by substituting the absorption coefficients reported by Higgs and Litovitz [10] into Eq. (12). Then the calculated relaxation time was substituted into Eq. (11) to obtain the value V_0. As shown in Fig. 7, the sound velocity of the alkali nitrates increases with decreasing size of the cation except in the case of $LiNO_3$. This result can be interpreted as follows. The sound velocity is a function of adiabatic compressibility and density as given by Eq. (2). The compressibility is governed by the packing fraction and the interactions among the constituent particles. An alkali nitrate can be regarded as an ionic liquid [11]. Ionic interaction, which is the most important among the interactions, depends largely on the spacing between ions, and increases with decreasing size of cation, if the ionic configuration does not vary significantly. On the other hand, the density of the alkali nitrate increases as the atomic weight of the cation increases. These facts qualitatively explain the results that the velocity of the alkali nitrate decreases with increasing size and atomic weight of the cation of the melt.

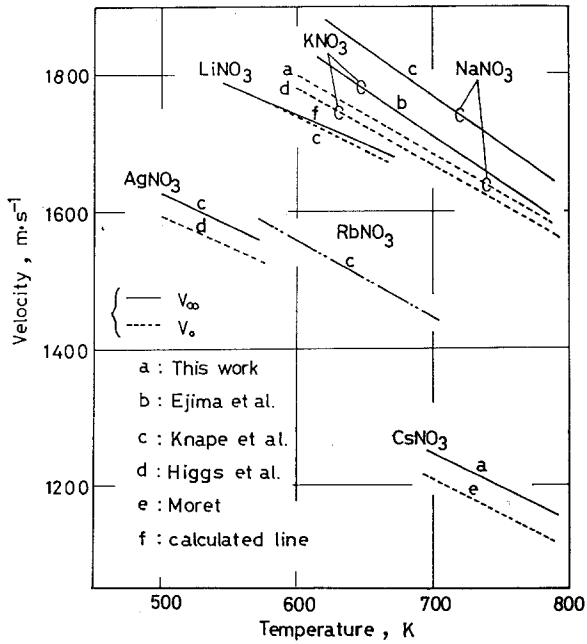

Fig. 7. Low-frequency sound velocity V_0 and limiting high-frequency sound velocity V_∞ in molten nitrates.

The sound velocity of $LiNO_3$ is less than that of KNO_3 despite the fact that the size and mass of the cation are the smallest of the alkali nitrates. This anomalous behavior can be explained as follows: The enthalpy and entropy on fusion of $LiNO_3$ are the largest among alkali nitrates, and the volume expansion of $LiNO_3$ at melting temperature is as large as 25%. These properties indicate that the packing fraction of $LiNO_3$ may be much smaller than the other alkali nitrates. Therefore, the velocity of $LiNO_3$ is smaller than the sodium and potassium nitrates, even though the size and mass of its cation are the smallest among alkali nitrates.

3.2. Hypersonic Velocities in $NaNO_3$–KNO_3 Binary Melts

Brillouin shifts of $NaNO_3$–KNO_3 binary melts were measured over the entire range of compositions at temperatures from the liquidus temperatures to 200 K above them. Hypersonic velocities were calculated from Brillouin shifts measured at scattering angles of 48.4, 86.6, and 135.8 deg. Sound velocities obtained at these angles agreed well with each other within the limits of experimental error.

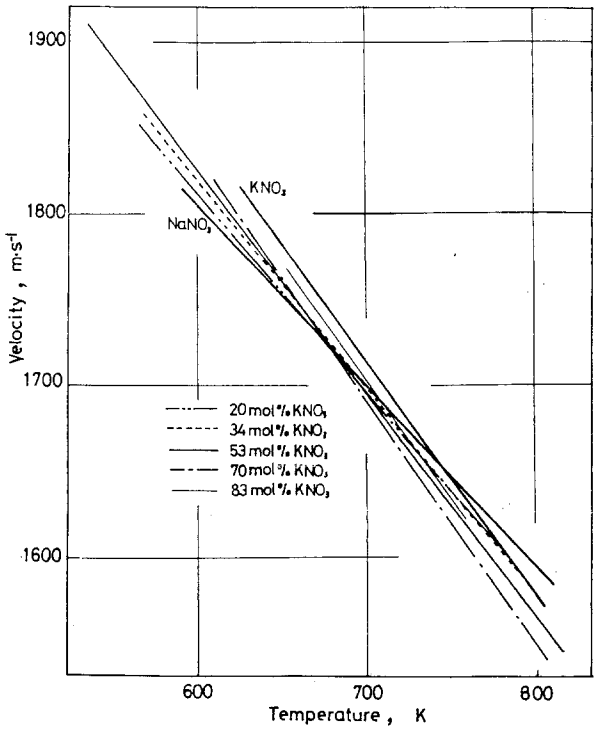

Fig. 8. Temperature dependence of hypersonic velocity for molten $NaNO_3$–KNO_3 binary system at 623 K.

Since the hypersonic velocity obtained decreases linearly with increasing temperature, linear equations representing the relation between hypersonic velocity and temperature at various compositions were correlated by the least squares method, and are shown in Fig. 8. In the temperature range from the liquidus to 680 K, the hypersonic velocity increases with increasing content of KNO_3, but the hypersonic velocities in molten $NaNO_3$ and KNO_3 become larger than those of the mixtures at temperatures above 740 K.

Hypersonic and ultrasonic velocities at 623 K are plotted against composition in Fig. 9. The line representing the composition dependence of hypersonic velocity shows a negative deviation from additivity. However, the extent of deviation is small, and is about 0.2% at the maximum. Similar negative deviations are also observed for the velocities at different temperatures.

The difference ΔV between hypersonic and ultrasonic velocities

$$\Delta V = V_{\text{hyper}} - V_{\text{ultra}} \tag{13}$$

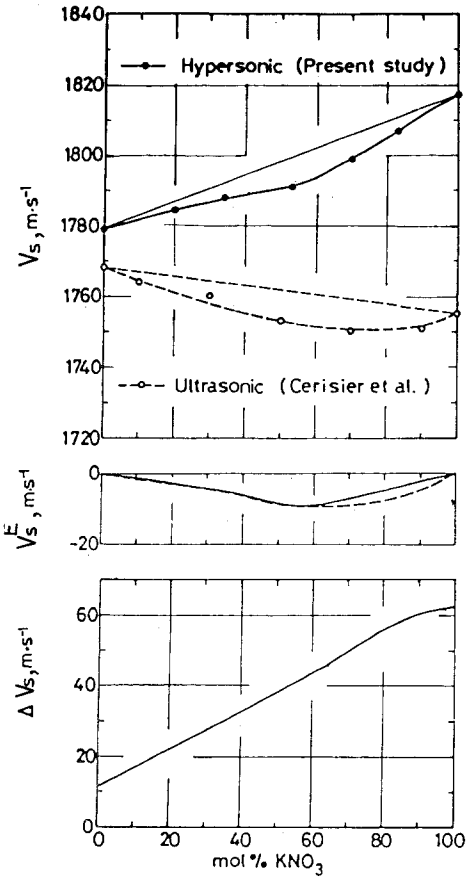

Fig. 9. Sound velocity V_s, its deviation V_s^E from additivity, and the difference ΔV_s between the hypersonic and the ultrasonic velocities for molten $NaNO_3$–KNO_3 binary system at 623 K.

is plotted against composition in Fig. 9. The value of ΔV is very small at compositions rich in $NaNO_3$. However, it increases as the content of KNO_3 increases, and exceeds 40 $m \cdot s^{-1}$ at compositions of more than 55 mole % KNO_3. This indicates that the relaxation time of the melt increases with increasing content of KNO_3.

The $NaNO_3$–KNO_3 binary melt consists of alkali cations and triangular NO_3^- anions. The cations and anions tend to form ion pairs to stabilize the Coulombic interaction. The ionic association may give the characteristics of alkali nitrates, namely lower melting point and smaller fusion enthalpy compared with alkali chlorides that belong to the class of typical ionic liquids.

Bond breaking and recombination of ions take place periodically in response to a cyclic pressure change caused by the propagation of sound waves. As the frequency of a sound wave becomes high, reconfiguration of ions to the equilibrium positions takes longer than the period of the corresponding pressure change, that is, a time lag called "structural relaxation" appears. The observed dispersion of sound propagation may result from the structural relaxation of associated species, namely ion pairs, formed in the melt.

For molten salts with common anions, the relaxation time becomes shorter, and the relaxation frequency becomes higher as the radius of the cation becomes smaller. Since the radius of the Na^+ ion (0.095 nm) is smaller than that of the K^+ ion (0.133 nm), the relaxation time becomes shorter and the relaxation frequency becomes higher for molten $NaNO_3$ than for molten KNO_3.

The experimental fact that the difference between hypersonic and ultrasonic velocity ΔV becomes larger at compositions rich in KNO_3 may be explained by the difference between the relaxation frequencies for the Na^+–NO_3^- pair and the K^+–NO_3^- pair. The dispersion of sound propagation caused by the structural relaxation becomes conspicuous as the content of KNO_3 increases, because the relaxation frequency of the K^+–NO_3^- pair is lower than the frequency range adopted in the present study.

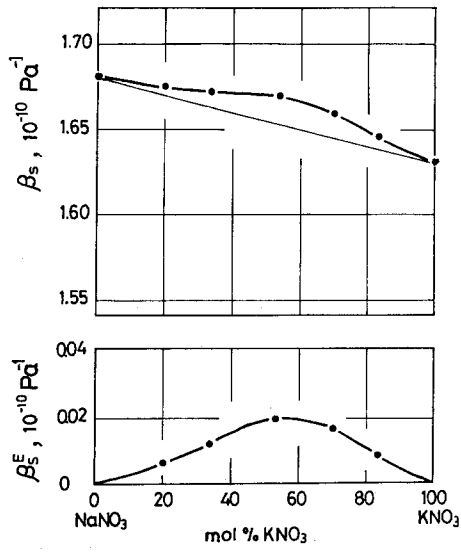

Fig. 10. Composition dependence of adiabatic compressibility β_s and its deviation β_s^E from additivity for molten $NaNO_3$–KNO_3 binary system at 623 K.

Adiabatic and isothermal compressibilities and constant-volume heat capacity were calculated from Eqs. (2)–(4) with the measured sound velocity. For the calculation of constant-volume heat capacity, it is necessary to use the constant-pressure heat capacity. However, the necessary data are not available in the literature. If additivity is assumed to be valid for the $NaNO_3$–KNO_3 binary system, the constant-pressure heat capacity at a certain composition can be calculated from the heat capacities of molten $NaNO_3$ and KNO_3. The values obtained in this way were used for the calculation of constant-volume heat capacity.

Adiabatic and isothermal compressibilities obtained are expressed by quadratic equations in temperature, and show small, positive deviation from additivity in contrast to the sound velocity, as shown in Figs. 10 and 11. Sternberg and Vasilescu [1] classified molten salts in terms of the excess isothermal compressibility β_t^E, which is the deviation from additivity. The value of β_t^E for a melt of nearly ideal mixing is small and positive, but that for a melt containing associated ions, such as molten $MgCl_2$, is large and positive. For such a system as $ZnCl_2$, in which bond breaking takes place on mixing with alkali halides, the value of β_t^E becomes negative. According to the classification proposed by Sternberg and Vasilescu, the $NaNO_3$–KNO_3 binary melt belongs to the class of nearly ideal mixing.

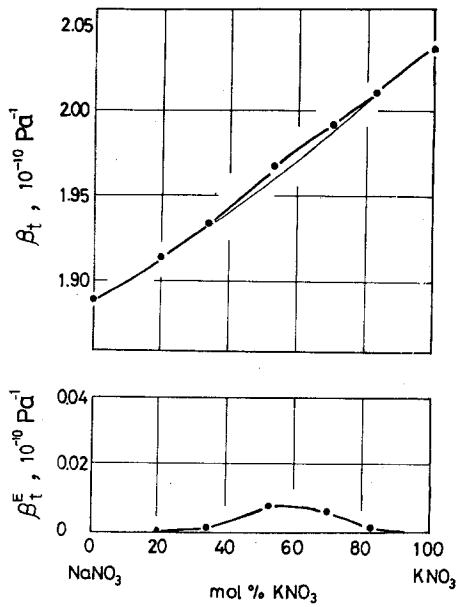

Fig. 11. Composition dependence of isothermal compressibility β_t and its deviation β_s^E from additivity for molten $NaNO_3$–KNO_3 binary system at 623 K.

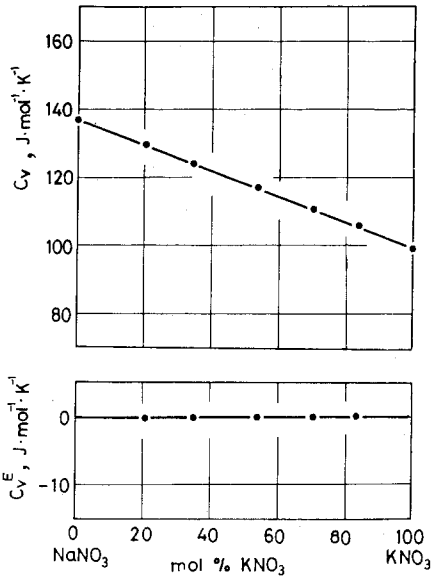

Fig. 12. Composition dependence of molar heat capacity at constant volume C_v and its deviation C_v^E from additivity for molten $NaNO_3$–KNO_3 binary system at 623 K.

The calculated constant-volume heat capacity C_v is also expressed by a quadratic equation of temperature, and appears to have an additive property, as shown in Fig. 12.

The internal pressure, which is the change in internal energy followed by the volume change at a constant temperature, can be calculated from the determined isothermal compressibility. The internal pressure calculated

Table I. Classification of Liquids by the Internal Pressure near the Melting Point (P_{int}, 10^8 Pa)

Organic liquid[a] (at 298 K)		Ionic liquid[a]		Liquid metal[a]		Present data	
$(C_2H_5)_2O$	2.4	LiCl	13.0	Hg	13	$NaNO_3$	11.8
n-C_7H_{16}	2.5	NaCl	13.1	Zn	41	KNO_3	12.1
CCl_4	3.4	KCl	11.1	Cd	28	$CsNO_3$	10.6
C_6H_6	3.7	$PbCl_2$	15	Ag	86		
		$CdCl_2$	7.0	Cu	32		

[a] Data from the literature.

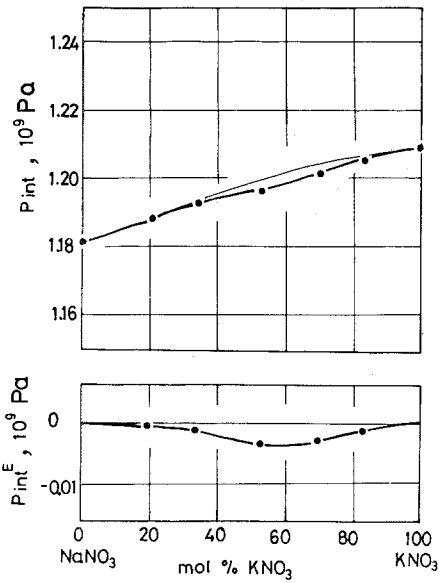

Fig. 13. Composition dependence of internal pressure P_{int} and its deviation P_{int}^{E} from additivity for molten $NaNO_3$–KNO_3 binary system at 623 K.

from Eq. (5) is shown in Table I and compared with those for the molecular, ionic, and metallic liquids. As is apparent from the table, the internal pressures of molten $NaNO_3$ and KNO_3 are about the same as those of typical ionic melts such as alkali chlorides. The internal pressure of the $NaNO_3$–KNO_3 binary melt increases as the content of KNO_3 increases. The deviation from additivity is small and negative, and is 0.25% at the maximum, as shown in Fig. 13. The $NaNO_3$–KNO_3 binary melt can be classified as a typical ionic liquid as far as the internal pressure is concerned, though such associated species as ion pairs exist in the melt to some extent.

4. CONCLUSION

Hypersonic velocities in molten single salts of $NaNO_3$, KNO_3, and $NaNO_3$–KNO_3 melts have been determined by means of Brillouin scattering spectroscopy over the entire range of compositions at temperatures from the liquidus temperatures to 200 K above them. From the hypersonic velocity obtained, such thermodynamic values as adiabatic and isothermal compressibilities, constant-volume heat capacity, and internal pressure were

calculated. The results obtained are summarized as follows:

1. Sound velocity decreases as the radius of the cation of the melt increases, with the exception of $LiNO_3$.

2. Dispersion of sound propagation is found in the the frequency range between ultrasonic and hypersonic waves for KNO_3 and $CsNO_3$.

3. Hypersonic velocity in the $NaNO_3$–KNO_3 binary melt decreases with increasing temperature, and its composition dependence shows small, negative deviations from additivity.

4. For the $NaNO_3$–KNO_3 binary melt, the difference between hypersonic and ultrasonic velocities increases as the content of KNO_3 increases, and becomes 40 $m \cdot s^{-1}$ or more, much larger than the limits of experimental error, at compositions above 55 mole % KNO_3. The observed dispersion of sound propagation is considered to be caused by structural relaxation of the ion pair.

5. Thermodynamic values calculated from the hypersonic velocity, such as adiabatic and isothermal compressibilities and constant-volume heat capacity, are expressed by quadratic correlations in temperature, and their composition dependences show an additive property, indicating that the melt can be treated as a nearly ideal mixture. On the other hand, the internal pressure calculated from the isothermal compressibility shows that the melt is classified as a typical ionic liquid.

6. From the results obtained, $NaNO_3$–KNO_3 binary melts are considered to be ionic liquids, though they contain a certain amount of associated species, namely ion pairs; as a whole, the melts can be treated as nearly ideal mixtures for the evaluation of general physicochemical properties.

REFERENCES

1. S. Sternberg and V. Vasilescu, *Rev. Roumaine Chim.* **21**:1457 (1976).
2. R. W. Higgs and T. A. Litovitz, *J. Acoust. Soc. Am.* **32**:1108 (1960).
3. K. Suzuki and Y. Fukushima, *Z. Naturforsch.* **32a**:1438 (1977).
4. L. Brillouin, *Compt. Rend.* **158**:1331 (1914).
5. L. M. Torell and H. E. G. Knape, *Z. Naturforsch.* **34a**:899 (1979); H. E. G. Knape and L. M. Torell, *J. Chem. Phys.* **62**:4111 (1975); R. Aronsson, H. E. G. Knape, and L. M. Torell, *J. Chem. Phys.* **68**:3794 (1978).
6. P. Cerisier, G. Finiels, and Y. Doucet, *J. Chim. Phys.* **6**:836 (1974).
7. J. O'M. Bockris and N. E. Richards, *Proc. Roy. Soc. London A* **241**:44 (1957).
8. J. M. Moret, Thesis, Université de Provence, Marseille (1975).
9. C. J. Montrose, V. A. Solovyev, and J. A. Litovitz, *J. Acoust. Soc. Am.* **43**:117 (1968).
10. R. W. Higgs and T. A. Litovitz, *J. Acoust. Soc. Am.* **32**:1208 (1960).
11. T. Ejima *et al.*, *J. Jpn. Inst. Metals* **46**:43 (1982).